analytical chemistry

Article

Ultra-High Mass Resolving Power, Mass Accuracy, and Dynamic Range MALDI Mass Spectrometry Imaging by 21-T FT-ICR MS

Andrew P. Bowman, Greg T. Blakney, Christopher L. Hendrickson, Shane R. Ellis, Ron M. A. Heeren,* and Donald F. Smith*

Cite This: *Anal. Chem.* 2020, 92, 3133–3142

Read Online

ACCESS | Metrics & More | Article Recommendations | Supporting Information

ABSTRACT: Detailed characterization of complex biological surfaces by matrix-assisted laser desorption/ionization (MALDI) mass spectrometry imaging (MSI) requires instrumentation that is capable of high mass resolving power, mass accuracy, and dynamic range. Fourier transform ion cyclotron resonance mass spectrometry (FT-ICR MS) offers the highest mass spectral performance for MALDI MSI experiments, and often reveals molecular features that are unresolved on lower performance instrumentation. Higher magnetic field strength improves all performance characteristics of FT-ICR; mass resolving power improves linearly, while mass accuracy and dynamic range improve quadratically with magnetic field strength. Here, MALDI MSI at 21T is demonstrated for the first time: mass resolving power in excess of 1 600 000 (at m/z 400), root-mean-square mass measurement accuracy below 100 ppb, and dynamic range per pixel over 500:1 were obtained from the direct analysis of biological tissue sections. Molecular features with m/z differences as small as 1.79 mDa were resolved and identified with high mass accuracy. These features allow for the separation and identification of lipids to the underlying structures of tissues. The unique molecular detail, accuracy, sensitivity, and dynamic range combined in a 21T MALDI FT-ICR MSI experiment enable researchers to visualize molecular structures in complex tissues that have remained hidden until now. The instrument described allows for future innovative, such as high-end studies to unravel the complexity of biological, geological, and engineered organic material surfaces with an unsurpassed detail.
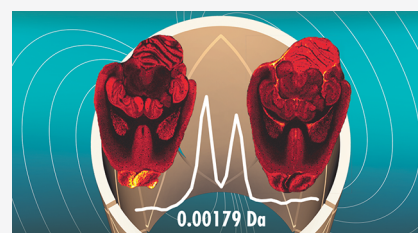
Mass spectrometry imaging (MSI) has proven to be a versatile tool, finding applications in a variety of fields including diseased tissue classification,[1-4] bacterial infections and resistance,[5,6] and drug metabolism.[7,8] The main strength of MSI is the ability to simultaneously reveal the spatial distributions of multiple molecules in a single experiment from complex biological materials, typically tissue sections.[9] However, the chemically complex samples typically analyzed bring challenges associated with the mass resolution and unambiguous assignment of the many different molecules detected. Due to this complexity, many signals are often unresolved from isobaric ions, such that generated ion images are not reflective of one unique molecule. This is a major hindrance to the study of the biochemical changes within tissues.

The most popular approach to begin addressing this complexity is the coupling of high mass resolving power and high mass accuracy analyzers with MSI ion sources, most commonly matrix-assisted laser desorption/ionization (MALDI).[10] This combination allows mass resolution of many isobaric ion species and direct assignment of elemental composition, thereby providing insight into the specific identities of the detected molecules. For lipids that are arguably the most widespread analyte class studies with MSI,[11-14] high mass resolving power and accuracy can facilitate true identification of sum-composition formula (i.e.,

lipid class and the combined number of carbons and double bonds across both fatty acyl chains), when sufficient to allow separation from isobaric interferences. In comparison to other biological molecules, resolving lipid complexity is further complicated by their relatively narrow mass range, with the majority of signals observed between m/z 700−900.[15] Lipids can further be observed as multiple adducts (e.g., addition of H^+, Na^+, K^+, OAc^-, or Cl^-, or loss of H^+) that are entangled with isotopes and other isobaric species. This results in a highly complex mass spectra that cannot be resolved with conventional high mass resolving power (e.g., $\leq$ 150 000 @ m/z 750).[15] Improvements in the achievable mass resolving of MSI technology is needed to unravel the spatial distributions of unique sum-composition lipid species that can have dramatically different biological functions

Fourier transform mass spectrometers; Fourier transform ion cyclotron resonance (FT-ICR) or orbital trapping (i.e., Orbitrap) offer higher mass resolving power and mass accuracy than other types of mass spectrometers (e.g., time-of-flight and

ion trap). FT-ICR mass spectrometers provide the highest mass resolving power and mass accuracy of any mass analyzer, with up to parts-per-billion (ppb) mass accuracy, high dynamic range, and mass resolving power values greater than 1 000 000 in routine analyses.[16−18] Mass resolution and sensitivity in FT-ICR instrumentation can also be improved by the use of absorption mode processing,[18,19] although this has not yet been widely exploited for MSI applications.[17] In a proof-of-principle study, absorption mode MALDI FT-ICR MSI on a 9.4 T system provided mass resolving powers in excess of 250 000 for lipid species observed from mouse brain tissue.[18,20] Several studies have shown similar high mass resolution on Orbitrap systems,[21−23] though additional difficulties introduced in imaging systems typically report lower overall mass resolution.[24−26] High mass resolution is necessary to distinguish both nominally isobaric lipids, where common mass differences of less than 10 mDa[15] occur, as well as isotopic interferences, where mass differences less than 3 mDa occur. While many lower field FT-ICR and Orbitrap instruments can distinguish the more common isobaric interferences, they are typically incapable of resolving mass differences less than 3 mDa.[27−29] More recently, desorption-electrospray ionization-MSI using a 7T FT-ICR system combined with absorption mode processing and external acquisition electronics demonstrated resolving powers up to 1 000 000 for lipid species.[17] However, the number of ions had to be reduced to avoid space-charge and peak coalescence effects, which reduced the dynamic range by 2 orders of magnitude, and the m/z range was truncated (m/z 765−832). Higher magnetic field strength mitigates these problems, and enables larger ion populations to be analyzed, for high dynamic range broadband spectra at high mass resolution. The method described for DESI at 7 T helps overcome a key challenge in FT-ICR MSI by increasing the transient length while minimizing acquisition overhead, helping to balance the desired mass resolution with practical acquisition times for experiments that typically involve acquisitions of tens of thousands of spectra. These practical acquisition times are paramount within MALDI imaging, where the use of volatile matrices limits how long any single experiment can be performed before the matrix sublimes from the sample.

Outside of the improvements offered by absorption mode data processing, analysis times can be reduced by increasing the strength of the magnet used for FT-ICR. Mass resolution increases linearly with magnetic field strength,[30] allowing for decreases in transient length without sacrificing resolving power. In the context of typically long MSI acquisition times, this improvement can reduce experimental times by several hours, a significant increase in throughput. Multiple frequency detection promises an increase in mass resolving power that scales linearly with the frequency order multiple.[31] However, to date this technique has not been applied to mass spectrometry imaging, though significant progress has been shown in ESI-based methods, which have reported mass resolving power of more than 10 000 000 in the lipid range.[16,21,32]

The key parameters of FT-ICR that vary with magnetic field strength (dynamic range, mass accuracy, and ion-number induced frequency fluctuations) are especially important in MSI, due to the changes in ion yield depending on tissue type,[33] as well as a lack of control (e.g., via automatic gain control) over the number of ions entering the analyzer cell at each pixel. Further, the rich information available within the lipid range sees an enormous benefit from higher magnetic

fields, in part from the biological dynamic range of lipids, but also from the number of nominally isobaric peaks possible in biological tissues. The advantage of increased mass resolution is obvious, but the improvement to mass accuracy and dynamic range can be crucial. High mass accuracy over long analysis times is important to generate highly accurate MSI images, as any drift in mass across an experiment would necessitate either pixel-to-pixel correction for this drift, or wider mass selection windows for image generation to encapsulate the ion as its apparent m/z shifts over time. High-field FT-ICR mass spectrometers offer external mass calibrations of less than 0.2 ppm (ppm),[34] and internal calibration less than 0.1 ppm.[35] High dynamic range is a key performance metric for MSI, given the wide dynamic range of lipid concentrations,[36] and differences in the ionization efficiencies of these biomolecules. Increased dynamic range is important to distinguish low abundance species while still detecting highly abundant lipids without distortion in relative ion abundances. The higher the magnetic field of an FT-ICR, the less susceptible it is to ion-number induced frequency shifts, which can hinder identification of peaks and complicate calibration of data sets, as has been described previously.[37−39]

Within the field of lipidomics, both shotgun and LC-MS based methodologies have achieved mass resolution in the lipid range greater than 100 000 along with sub-ppm mass accuracy, enabling assignment of 200−500 lipids in a single experiment.[40−42] Due to the increased fluctuations in signal intensity inherent to MSI, progress toward such endeavors is slower, success has been shown in a variety of FT based instruments with numerous ionization techniques, including Liquid Extraction Surface Analysis,[43] MALDI,[44] DESI,[17] and LAESI.[20] LAESI was performed on a 21 T FT-ICR mass spectrometer which separated the isotopic fine structure of nominally overlapping metabolites of plant leaves, which improved identification by utilizing multiple peaks per metabolite in the identification process. Additionally, the experimental time frame for the 21 T is significantly reduced compared to other instruments with similar mass resolution, without sacrificing either signal magnitude or mass range, as has been attempted with lower-field instruments.[17,20,35]

In this work, we evaluate for the first time the performance of MALDI MSI combined with 21 T FT-ICR MS for biological tissue imaging, as well as the use of automated annotation to begin exploring the highly complex information available from such experiments. In particular, we demonstrate (i) the combined higher mass resolving power and mass accuracy with the stability of these parameters across long MSI experiments; (ii) increased biochemical information obtained during MALDI MSI facilitated by the high mass resolving power and mass accuracy; (iii) single-pixel dynamic range exceeding 500:1, which enables imaging and identification of very low abundance ions; (iv) automated analytical tools to identify potentially hundreds of lipids utilizing thousands of peaks. Combined, this work demonstrates the high potential of MALDI MSI and 21 T FT-ICR for studying localized biomolecular processes within tissues and their disease-induced alterations.

■ METHODS

Materials. Methanol (LC-MS grade), ethanol (LC-MS grade), xylene (LC-MS grade), water (LC-MS grade), anhydrous chloroform (≥99.9% purity), and crystalline norharmane (9H-β-carboline) were purchased from Sigma-
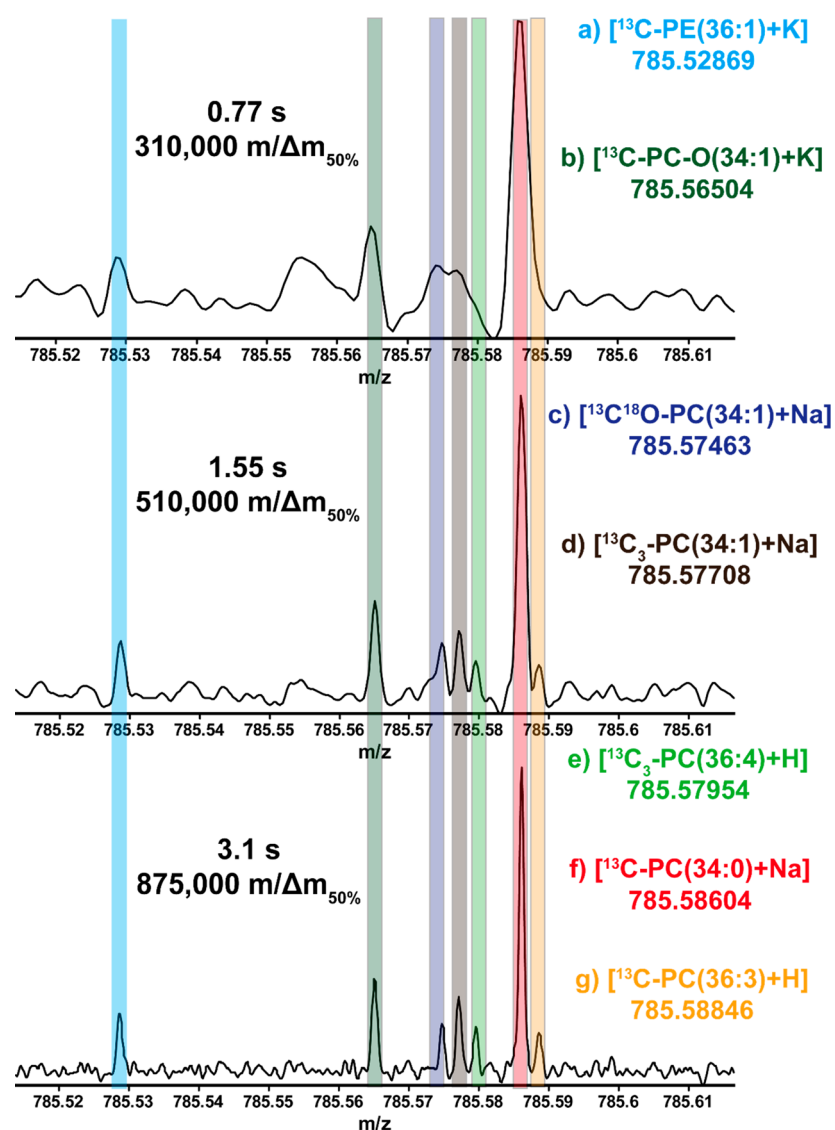
Figure 1. Mass resolution and sensitivity improve with longer transient length. Within a 100 mDa mass range, seven different peaks are detected, which belong to six different lipid species. Of these, five are unresolved at 0.77 s. While distinguishable at 1.55 s, all seven peaks are fully resolved only at 3.1 s transient. These seven peaks correspond to the isotopologues of the monoisotopic species, typically the ^{13}C ion, as in (a), (b), (f), and (g). Other species are also present, corresponding to the $^{13}C_3$ isotopologue, as in (d) and (e). The $^{18}O^{13}C$ isotopologue of $[PC(34:1)+Na]^+$ is also resolved (c) from the $^{13}C_3$ isotopologue of the same parent species.

Aldrich (Zwijndrecht, The Netherlands) and used without further purification. Indium tin oxide (ITO)-coated glass slides were purchased from Delta Technologies (Loveland, CO).

Biological Samples. Healthy rat brain was obtained from Maastricht University in accordance with protocols approved by the Animal Care and Use Committee under Animal Experiment Committee (DEC) number 2016−006 AVD107002016720. Four transverse rat brain segments (12 μm thick) were sectioned with a cryo-microtome at −20 °C and thaw-mounted on ITO-coated glass slides. Some distortion of the tissue sections occurred during the mounting process.

Sample Preparation. Norharmane matrix (7 mg/mL) in CHCl3:MeOH (2:1 v/v) was applied to the tissue with a TM-Sprayer (HTX Technologies, Chapel Hill, NC). Spray conditions were as follows: flow rate, 0.12 mL/min; N2 pressure, 10 psi; N2 temperature, 30 °C; spray-head velocity,

1200 mm/min; track spacing, 3 mm; number of layers, 15; drying time between layers, 30 s.

Instrumentation. All MSI experiments were performed on a hybrid linear ion trap 21 T FT-ICR mass spectrometer at the National High Magnetic Field Laboratory (NHMFL) at Florida State University (Tallahassee, FL). A Velos Pro linear ion trap (Thermo Scientific, San Jose, CA) was combined with NHMFL-designed external linear quadrupole ion trap, quadrupole ion transfer optics, and a novel dynamically harmonized ICR cell, which is operated at 7.5-V trapping potential.[34] Briefly, the cell uses 120° cell segments for ion excitation and detection, for improved excitation electric field, detection sensitivity, and reduced third harmonic signals.[45,46]

The commercial ion source and stacked ring ion guide were replaced with an elevated-pressure MALDI ion source incorporating a dual-ion funnel interface (Spectroglyph LLC, Kennewick, WA) as has been described previously.[47] Voltages within the funnels were 625 kHz, 150 V peak-to-peak (first,
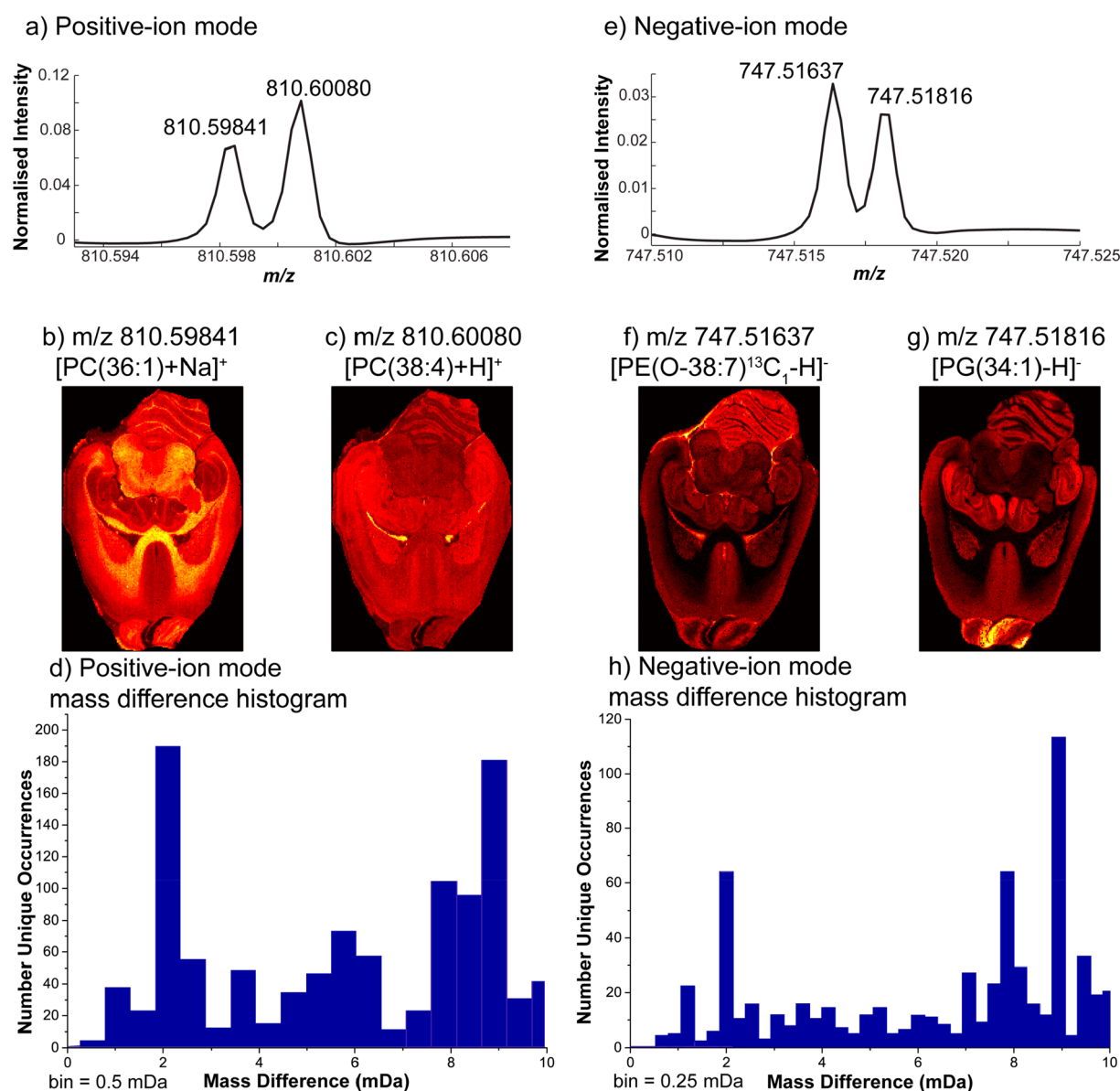
Figure 2. Representative images of close mass differences in negative and positive mode, from a single, scan. Images are total ion current normalized. Positive mode lipid spectra have a significant number of mass differences of 2.4 mDa (a), representing the difference between $^{12}C_2$ and $^{23}Na^1H$. 2.4 mDa differences are baseline resolved, and show significantly different distributions within brain tissue (b and c). There are nearly 200 such differences in the averaged spectra, shown in 0.5 mDa bins (d). Similarly, negative mode spectra have 1.79 mDa mass differences (e). These 1.79 mDa differences are resolved to better than full-width half-maximum, differentiated well enough to distinguish them in brain tissue (f and g). The of 1.79 mDa mass difference is relatively uncommon in negative mode, but mass differences of 10 mDa or less occur approximately 500 times in the averaged spectra, shown in 0.25 mDa bins (h).

high-pressure ion funnel), and 1.2 MHz, 90 V peak-to-peak (second, low-pressure ion funnel). An electric field gradient of ~10 Vcm^{-1} was maintained within the dual-funnel system, with a gradient of 100 Vcm^{-1} between the sample and the funnel inlet. The system was equipped with a Q-switched, frequency-tripled Nd:YLF laser emitting 349 nm light (Explorer One, Spectra Physics, Mountain View, CA). The laser was operated at a repetition rate of 1 kHz and pulse energy of ~1.2 μJ. Pressure within the ion source was set to 10 mbar in the first ion funnel, and 2 mbar in the second ion funnel. MALDI stage motion was synchronized with ion accumulation using the Velos trigger signal indicating commencement of the ion trap injection event, as previously described.[47] The mass spectrometer was operated with an ion

injection time of 250 ms and automatic gain control (AGC) was turned off. A transient duration of 3.1 s was used for ultrahigh mass resolving power analyses, resulting in a total time of 4s per pixel. Spectra were obtained in both positive and negative mode, at 100 μm spatial resolution. Total number of pixels per brain section were approximately 22 000, and 24 h of experimental time. A Predator data station was used for ion excitation and detection.[48]

Data Processing and analysis. Absorption mode mass spectra were generated by phase correction of the time domain transients,[49] and peaks with a signal magnitude greater than 6 times the standard deviation of the baseline root-mean-square (RMS) noise were exported to peak lists. Mass calibration was performed on known lipid species, with a wide range of
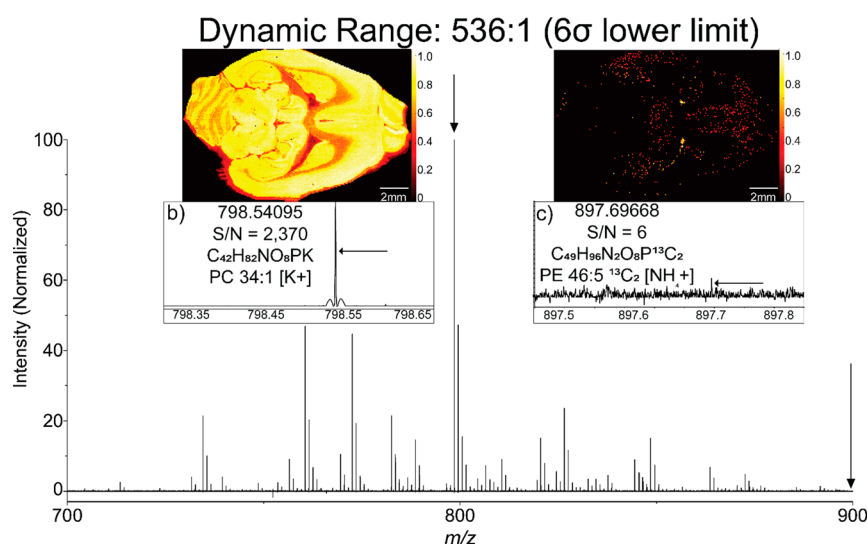
Figure 3. Single on-tissue mass spectrum illustrates high dynamic range per pixel. Peaks were picked at a threshold of six standard deviations above the baseline noise. Dynamic range in a single average pixel of at 536:1 is demonstrated here at pixel number 10 000, (a). Mass scale expanded segment around most abundant peak $[PC\ 34:1 + K]^+$ (b). Further, peak at 798.5410 generates a bright image (b). One of the lowest S/N peaks, the $^{13}C_2$ isotope of $[PE\ 46:5 + H]^+$ (c) while less clear, still yields informative molecular images, being highlighted especially in the ventricles (images are TIC normalized).

spectral intensities ($[PC\ 34:1 + K]^+$, $[SM\ 34:1;2 + H]^+$, $[PE\ 36:4\ ^{13}C + H]^+$, $[PC\ 32:0 + Na]^+$, $[PC\ 34:1 + H]^+$, $[PC\ 38:4 + Na]^+$, and $[PC\ 38:4 + K]^+$) and the data were converted to imzML format using in-house Matlab routines, msconvert from the ProteoWizard software suite (version 3.0.11537),[50] and imzMLConverter version 1.3.[51] The ALEX[123] software package was used for sum-composition lipid identification at a search tolerance of 1 mDa.[41,52] All phospholipid classes were chosen, as were sphingolipids and glycerolipids, with chain-lengths of 14 carbons or greater. Adducts were limited to H^+, Na^+, and K^+, and negative mode was restricted here to simple loss of H^+. Images generated are normalized to the total ion current per pixel (TIC).

RESULTS AND DISCUSSION

High Mass Resolving Power. To assess the benefits of performing 21 T MALDI MSI in terms of mass resolving power, we analyzed rat brain sections in both positive and negative ion mode using different transient acquisition times. Figure 1 shows the achieved mass resolving power in the positive-ion mode using 0.76, 1.55, and 3.1 s transients within the m/z range 785.52−785.6. Increasing mass resolution shows increasing spectral complexity, as five peaks are resolved from what first appears to be only two, with two additional peaks within 100 mDa which were sufficiently distinct to be identified at all transient lengths. We annotated the seven peaks within this region as belonging to six different species of lipids: $[PE(36:1)+K]^+$, $[PC-O(34:1)+K]^+$, $[PC(34:1)+Na]^+$, $[PC(36:4)+H]^+$, $[PC(34:0)+Na]^+$, and $[PC(36:3)+H]^+$. Of these, four are the $^{13}C_1$ isotope: ($[PE(36:1)+^{13}C+K]^+$, $[PC-O(34:1)+^{13}C+K]^+$, $[PC(34:0)+^{13}C+Na]^+$, and $[PC(36:3)+^{13}C+H]^+$), two are the $^{13}C_3$ isotope ($[PC(34:1)+\ ^{13}C_3+Na]^+$ and $[PC(36:4)+\ ^{13}C_3+H]^+$), and the final peak is the $^{13}C^{18}O$ isotope ($[PC(34:1)+\ ^{13}C^{18}O+Na]^+$). These peaks show mass accuracy errors between −50 and 13 parts-per-billion (ppb). Additionally, isotope ratios in the summed average spectra deviate <15% from theoretical in these seven peaks (SI Figure 1), offering additional certainty in that correct sum-composition identification has been made, as well that there are no convoluted peaks being presented as a single peak. Deviation from the expected 2-fold improvement in mass resolving power upon doubling of the transient duration is due to known collisional damping during the detection event.[34] Current work focuses on a solution to limit transmission of the neutral buffer gas in the external accumulation multipole to the ultrahigh vacuum region. Recently, a mass resolving power of ~600 000 (at m/z 760) for MALDI MSI on a 15 T FT-ICR MS (the highest commercially magnetic field available for FT-ICR) was reported. This value also deviates from the theoretical mass resolving power for a 5.2 s transient (magnitude mode), which is ~788 000.[53]

To further assess the utility of the 21 T, we analyzed the data set for peaks with close neighbors (here defined as <10 mDa). We extracted the 3.1 s transient from a single pixel (number 10 000) as a representative spectrum from each data set. In positive-ion mode, a difference of 0.0024 Da (2.4 mDa) at m/z 810 was present (Figure 2a), representing the difference between Na_1H_1 versus C_2 (the addition of two carbon atoms and three double bonds to the lipid fatty acid chains) which requires a mass resolving power ($m/\Delta m_{50\%}$) of 337 000 at m/z 810 to resolve. These two ions were well resolved, and lipid identities were assigned $[PC(36:1)+Na]^+$ and $[PC(38:4+H)]^+$ with high confidence (100 ppb, see discussion below). Each species had very different spatial distributions, with the former ($[PC(36:1)+Na]^+$) being relatively evenly distributed (Figure 2b), while the latter ($[PC(38:4+H)]^+$) had higher abundance in the lateral ventricle (Figure 2c). The higher abundance of $[PC(38:4)+Na]^+$ in the ventricles matches with its role as a pro-inflammatory cytokine.[54] Interestingly, such a small mass difference was not uncommon, with a mass difference of 2.4 mDa observed over 190 times in any single pixel spectrum, and more than 1 000 000 times over a single MSI experiment (Figure 2d). Without sufficient mass resolving power, any one of the images of these ~190 pairs of closely spaced ions could yield incorrect assignments and yield a summed spatial distribution reflective of neither individual species. A variety

of other recurrent mass differences can be detected in the single spectra, ranging from 1 to 10 mDa, including isotopic patterns (e.g., $^{13}C_2$ vs H_2 is a difference of 8.94 mDa). The change in $^{13}C_2$ vs H_2 is an important one, as this denotes the possible overlap for species that differ by a single double bond (i.e., as PC(34:1) to PC(34:0)). Single unsaturation changes have been shown to be important in various types of disease states, including cancers[55,56] and multiple sclerosis,[57] and so the ability to resolve such fine mass differences opens the door to studying the precise roles of the subtle changes in lipid structure throughout tissues.

Using the same experimental design in the negative-ion mode, additional small mass differences could be resolved. For example, a mass difference of 0.00179 Da (1.79 mDa) at m/z 757.52 was observed at 31 different masses. This corresponds the mass difference of $C_2N_1{}^{13}C_1$ versus H_3O_3 (Figure 2e). While less common than the NaH vs C_2 mass difference in positive mode, ether-linked phosphatidylethanolamine (PE) and PC lipids can have this difference from the phosphatidyl-glycerol (PG) class. These peaks were thus identified as phosphatidylethanolamine $[PE(O\text{-}38:7)+{}^{13}C-H]^-$ and $[PG(34:1)\text{-}H]^-$. This is the smallest mass difference observed in any MSI data set to date. The PE is a ^{13}C-containing nuclide of the monoisotopic PE lipid at m/z 746.51300. PE and PG lipids are synthesized by different biological pathways and have different physiological function. PE lipids are ~20% of all phospholipids, and are especially abundant in white matter of the cerebellum (Figure 2f).[58] By contrast, PG lipids are associated with ATP-Binding Cassette 3, though what transport function is utilized is unknown.[59] The 1.79 mDa mass difference occurred over 100 000 times in our MSI experiment, with 33 unique pairs detected in the total mass spectrum. As in the positive mode, the $^{13}C_2$ vs H_2 difference occurs regularly, and has many of the same ramifications as discussed above.

Dynamic Range. One of the most problematic complications in MSI is the low relative ionization efficiency from the surface, which combined with the wide range of analyte concentrations, places significant demands on the single scan dynamic range achievable in an MSI experiment. High sensitivity and dynamic range are thus necessary to detect low abundance and/or poorly ionized species without distorting the peak abundances obtained from high intensity signals. Figure 3a shows a single pixel mass spectrum of the lipid m/z range from the positive-ion mode data set (scan no. 10 000), which has a dynamic range of 536:1 (expanded mass range spectrum shown in SI Figure 2). The dynamic range was calculated by dividing the signal magnitude of the base peak by the peak detection threshold of six standard deviations (6σ) above the baseline noise. As typically observed from brain tissue, the $[M+K]^+$ ion of PC(34:1) generated the highest signal magnitude, with a signal-to-noise = 2370:1 (Figure 3b; side lobe artifacts are a result of the absorption mode processing, and current work is focused on their removal). By contrast, rat brain tissue sections prepared from the same original organ and under the same conditions showed a signal-to-noise = 336:1 on a Thermo Orbitrap Elite set at 240 000 resolving power (@ m/z 400) at the Maastricht MultiModal Molecular Imaging Institute (data not shown). Using a peak detection threshold of 6σ above the baseline noise, the lowest intensity signal was observed with a signal-to-noise = 6 and corresponded to the $(PE(46:5)+{}^{13}C_2+H)+$ (Figure 3c). SI Figure 3 shows the isotopic distribution for PE 46:5, where the

$^{13}C_2$ containing nuclide can be identified at M+2. In addition, SI Figure 4 shows ppm error distributions for the monoisotopic peak, M+1 $({}^{13}C_1)$, and M+2 $({}^{13}C_2)$ which show good mass accuracy, despite the low S/N of the M+2 peak. Per pixel, the average dynamic range in positive ion mode was 438:1, with a maximum dynamic range of 2090:1 and a minimum of 60:1 (SI Figure 5). Negative-ion mode spectra had lower signal magnitude than positive mode, limiting the average dynamic range to 214:1, with a maximum of 849:1 and minimum of 30:1 (SI Figure 6).

High Mass Accuracy. FT-ICR MSI at 21 T showed a root-mean-square (rms) mass measurement accuracy of 62.12 ppb (Figure 4a), over 2-fold lower rms mass accuracy achieved on a
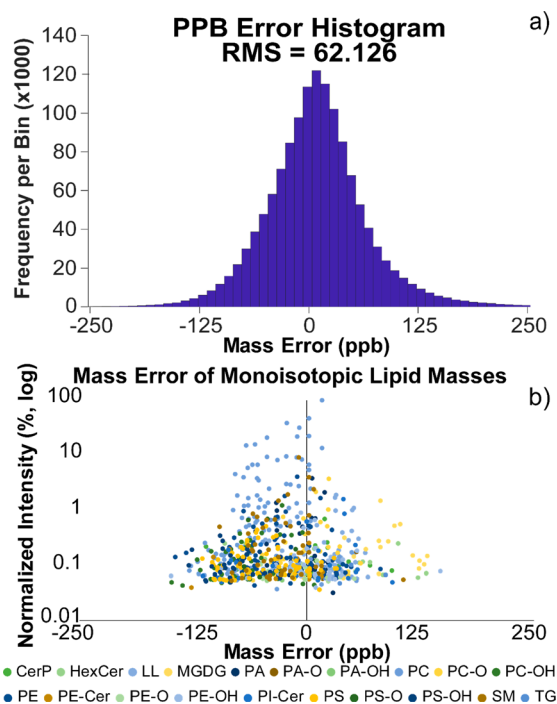
Figure 4. Error histogram and average mass error of tentatively identified lipids after internal calibration. Measured mass error histogram of 139 phosphatidylcholine lipids; the rms error is 61.12 ppb. Bin size = 10 ppb. (a), Lipid identifications by class. A tolerance of ±250 ppb results in 702 potential lipids identified within 150 ppb of their expected mass (b).

9 T instrument, which was limited to an rms of 158 ppb.[60] The center of the distribution is centered near zero, and the low standard deviation indicates low m/z fluctuation during the imaging experiment. SI Figure 7 shows the measured m/z variation for $[PC(36:1)+H]^+$ (m/z = 788.61638, dotted red line indicates the exact m/z) over the imaging experiment, where the maximum m/z deviation is 0.00018, with a standard deviation of 0.00078. Internal calibration was performed using seven tentatively identified lipid masses ($[PC(34:1)+K]^+$, $[SM(34:1;2)+H]^+$, $[PE(36:4)+{}^{13}C+H]^+$, $[PC(32:0)+Na]^+$, $[PC(34:1)+H]^+$, $[PC(38:4)+Na]^+$, and $[PC(38:4)+K]^+$). After this internal calibration, all scans were summed (in the mass domain), which generated an initial peak list of 2,643 above the 6σ noise limit. This list was then submitted to ALEX123 for identification. We tentatively identify 702 monoisotopic lipid peaks in positive-ion mode, which all have mass accuracy values of ±150 ppb (Figure 4b). These 702 lipid peaks correspond to 388 unique lipid IDs, after accounting for
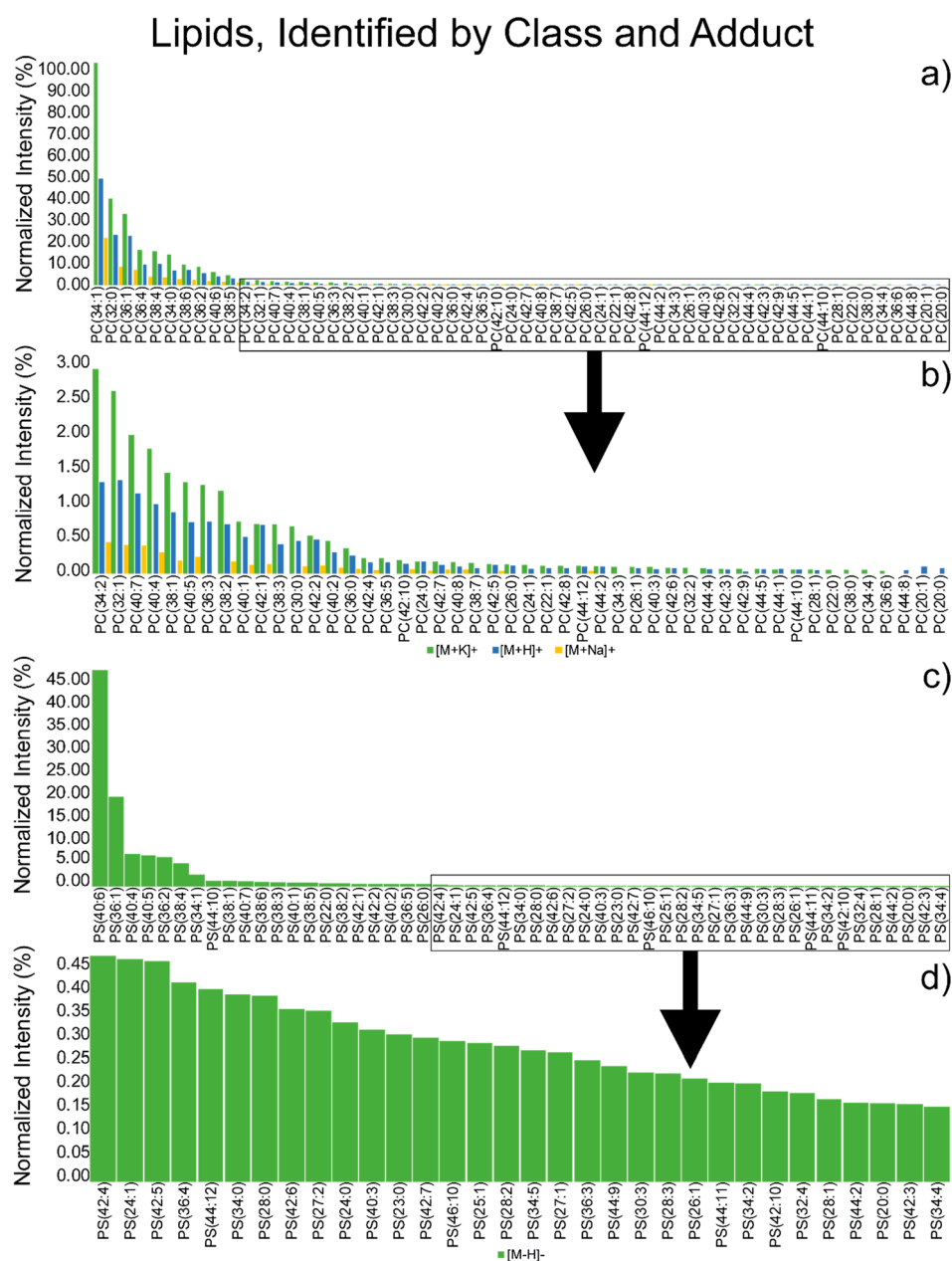
Figure 5. Relative abundance of identified lipids by cation and anion for selected classes. In the positive mode, the three major cations (proton, sodium, and potassium) are aligned next to one another, showing the same relative percentages between species, from the most abundant species (PC 34:1) and the other PCs above 3% (a), as well as for the lower abundant species down to the least abundant species with all three cations represented, PC 44:12 (b). The relative ionization rate between K⁺, H⁺, and Na⁺ hold strictly true down to 1.5%, and generally true down to 0.05%. While the dynamic range is lower for negative mode, we see many potential identifications for many lipid classes (c). We further observe a similar ability to identify potential lipids as low as 0.15% of the most abundant peak (PI 38:4), for a range of nearly three orders of magnitude from the summed spectra (d).

three possible cations types, which accounts for 26.9% of the initial peak list. SI Table 1 contains a full list of these lipids. An additional 1400 spectral peaks are as isotopologues (typically ^{13}C and $^{13}C_2$) of the 702 lipids, which accounts for ~80% of all peaks. Negative ion mode yielded similar results, where 662 potential monoisotopic lipid peaks (34%) were identified out of an initial peak list of 1927. Due to the lower S/N of the negative mode spectra, only 738 further peaks were identified as isotopes, for a total of ~72.6% of all peaks identified.

These lipid IDs are supported both by the high mass accuracy (<150 ppb, most <100 ppb) and in the positive mode by the intensity of multiple cations for the same species,

relative to one another (Figure 5a). As protonation, sodiation, and potassiation are all potentially available in brain MSI, we examined the potential to confirm our lipid identifications by comparing all three cations. For the most abundant lipid (PC(34:1)), the [M+K] ion has an average ppb error of 16.7, [M + Na] −43.5, and [M + H] 2.2. While these mass errors are low enough individually to be highly confident in their assignment, having all three ions within 60 ppb of one another provides another layer of certainty. Additionally, we can examine the normalized peak intensities of all three ions to one another, in this case showing 100%, 47.9%, and 21.4%, simplified to a ratio of 4.7:2.2:1. While this insight is not

necessarily informative on its own, we can compare this ratio to other PCs, with all the PCs above 3% of the base peak showing the same ratio (Figure 5a). Further, PCs that vary in relative intensity down to 0.2% of the base peak have generally similar ratios to PC(34:1), although as the intensities begin to approach the 6σ limit, the ratios begin to deviate and be less similar (Figure 5b). One likely scenario for this discrepancy at low S/N is that as peaks for any given scan drop below the 6σ threshold, the least abundant ions are ignored, leading to sum signal magnitudes in the averaged spectrum that are slightly erroneous. However, as the relative ratios of the three cations are invariable across three orders of magnitude, it improves our certainty that each identification is correct for all lipids within that class. While we observe no alterations to this ratio in the abundant lipid classes, theoretically alterations to this standard ratio could indicate greater abundance of a given lipid within different brain structures (i.e., within the ventricle space rather than within gray or white matter). It is worthwhile to further explore the potentials here, and whether there are observable changes to this ratio between other brain tissues. Additionally, we observe that other lipid classes show similar, though slightly different ratios (SI Figure 8), potentially related to the changes in brain tissue. Negative ionization does not typically have multiple ions of the same species (with deprotonation being the only common method of generating lipid anions unless dopants are added[61,62]); however, between the most abundant phosphatidylserine (PS(40:6)) and the least abundant (PS(34:4)) there is only a change in ppb error of 17.3 despite a change in intensity of more than an order of magnitude (Figure 5c).

CONCLUSION

We have demonstrated the utility of combining MSI workflows with a 21 T FT-ICR mass spectrometer. The high magnetic field, combined with a state-of-the-art ICR cell design provides ultrahigh mass resolving power, ppb mass measurement accuracy, and high sensitivity for molecular imaging studies. This advanced instrumentation will pave the way for better understanding of the molecular structure of many tissue types, as well as clarifying current ambiguities in MSI. The unique capabilities of this instrument have not yet been fully utilized: online tandem mass spectrometry is possible via collision induced dissociation in the linear ion trap, or in the ICR cell via infrared multiphoton dissociation or ultraviolet photo dissociation. Further, the use of harmonic detection cells would further increase the speed of acquisition in these experiments or allow for even higher mass resolving power in a similar time frame. Combined with data-driven MSI acquisition techniques (such as Data-Dependent Acquisition), this instrument promises the most information per unit time of any MSI platform. The estimated number of charges sent to the ICR cell in these experiments is $\sim 4 \times 10^5$, based on the mass spectral calibration parameters. The 21T FT-ICR routinely operates with ion targets of $1-3 \times 10^6$, so additional improvement in dynamic range per pixel is expected. Further, we aim to leverage the unique capabilities of this instrument for other biomolecule imaging experiments, such as metabolites, tryptic peptides, and intact proteins.. This instrument will provide valuable insight into the molecular complexity of tissues at an unprecedented mass spectral resolution, allowing for greater insight into the true distribution of all molecules, as well as accelerating the identification of subtle changes hidden within tissues.

ASSOCIATED CONTENT

ⓈI Supporting Information

The Supporting Information is available free of charge at https://pubs.acs.org/doi/10.1021/acs.analchem.9b04768.

Eight additional figures as described in the text and table with a complete list of all tentatively identified lipid species (PDF)

AUTHOR INFORMATION

Corresponding Authors

Ron M. A. Heeren − Maastricht MultiModal Molecular Imaging (M4I) Institute, Division of Imaging Mass Spectrometry (IMS), Maastricht University, Maastricht 6629ER, The Netherlands; ⓞ orcid.org/0000-0002-6533-7179; Email: r.heeren@maastrichtuniversity.nl

Donald F. Smith − National High Magnetic Field Laboratory, Florida State University, Tallahassee, Florida 32310-4005, United States; ⓞ orcid.org/0000-0003-3331-0526; Email: donsmith@magnet.fsu.edu

Authors

Andrew P. Bowman − Maastricht MultiModal Molecular Imaging (M4I) Institute, Division of Imaging Mass Spectrometry (IMS), Maastricht University, Maastricht 6629ER, The Netherlands

Greg T. Blakney − Maastricht MultiModal Molecular Imaging (M4I) Institute, Division of Imaging Mass Spectrometry (IMS), Maastricht University, Maastricht 6629ER, The Netherlands; ⓞ orcid.org/0000-0002-4205-9866

Christopher L. Hendrickson − National High Magnetic Field Laboratory and Department of Chemistry and Biochemistry, Florida State University, Tallahassee, Florida 32310-4005, United States

Shane R. Ellis − Maastricht MultiModal Molecular Imaging (M4I) Institute, Division of Imaging Mass Spectrometry (IMS), Maastricht University, Maastricht 6629ER, The Netherlands; ⓞ orcid.org/0000-0002-3326-5991

Complete contact information is available at:
https://pubs.acs.org/10.1021/acs.analchem.9b04768

Author Contributions

R.M.A.H. and D.F.S. conceived and coordinated the experiments. A.P.B., C.L.H., S.R.E., R.M.A.H., and D.F.S. designed the experiments. A.P.B., S.R.E., R.M.A.H., and D.F.S. carried out the MSI experiments. A.P.B., G.T.B., S.R.E., and D.F.S. conducted data processing and analysis. G.T.B., C.L.H., and R.M.A.H. provided feedback and quality control of MSI data. A.P.B., S.R.E., and D.F.S. wrote the manuscript, which was edited by all coauthors.

Notes

The authors declare no competing financial interest.

of Limburg. Part of this work was financially supported through the EURLIPIDS program of Euregio.

■ REFERENCES

(1) Vaysse, P. M.; Heeren, R. M. A.; Porta, T.; Balluff, B. *Analyst* **2017**, *142* (15), 2690−2712.

(2) Lazar, A. N.; Bich, C.; Panchal, M.; Desbenoit, N.; Petit, V. W.; Touboul, D.; Dauphinot, L.; Marquer, C.; Laprevote, O.; Brunelle, A.; Duyckaerts, C. *Acta Neuropathol.* **2013**, *125* (1), 133−44.

(3) Chaurand, P.; Schwartz, S. A.; Caprioli, R. M. *J. Proteome Res.* **2004**, *3* (2), 245−252.

(4) Chen, Y.; Allegood, J.; Liu, Y.; Wang, E.; Cachon-Gonzalez, B.; Cox, T. M.; Merrill, A. H., Jr.; Sullards, M. C. *Anal. Chem.* **2008**, *80* (8), 2780−8.

(5) Scott, A. J.; Post, J. M.; Lerner, R.; Ellis, S. R.; Lieberman, J.; Shirey, K. A.; Heeren, R. M. A.; Bindila, L.; Ernst, R. K. *Proc. Natl. Acad. Sci. U. S. A.* **2017**, *114* (47), 12596−12601.

(6) Hoefler, B. C.; Gorzelnik, K. V.; Yang, J. Y.; Hendricks, N.; Dorrestein, P. C.; Straight, P. D. *Proc. Natl. Acad. Sci. U. S. A.* **2012**, *109* (32), 13082−7.

(7) Schulz, S.; Becker, M.; Groseclose, M. R.; Schadt, S.; Hopf, C. *Curr. Opin. Biotechnol.* **2019**, *55*, 51−59.

(8) Castellino, S.; Groseclose, M. R.; Wagner, D. *Bioanalysis* **2011**, *3* (21), 2427−41.

(9) Ellis, S. R.; Bruinen, A. L.; Heeren, R. M. *Anal. Bioanal. Chem.* **2014**, *406* (5), 1275−89.

(10) Taban, I. M.; Altelaar, A. F. M.; Van der Burgt, Y. E. M.; McDonnell, L. A.; Heeren, R. M. A.; Fuchser, J.; Baykut, G. *J. Am. Soc. Mass Spectrom.* **2007**, *18* (1), 145−151.

(11) Bowman, A. P.; Heeren, R. M. A.; Ellis, S. R., Advances in mass spectrometry imaging enabling observation of localised lipid biochemistry within tissues. *TrAC, Trends Anal. Chem.* **2019**.120115197

(12) Zhao, C.; Xie, P. S.; Yang, T.; Wang, H. L.; Chung, A. C. K.; Cai, Z. W. *Chin. Chem. Lett.* **2018**, *29* (8), 1281−1283.

(13) Sugiyama, E.; Yao, I.; Setou, M. *Biochem. Biophys. Res. Commun.* **2018**, *495* (1), 1048−1054.

(14) Sans, M.; Feider, C. L.; Eberlin, L. S. *Curr. Opin. Chem. Biol.* **2018**, *42*, 138−146.

(15) Bielow, C.; Mastrobuoni, G.; Orioli, M.; Kempa, S. *Anal. Chem.* **2017**, *89* (5), 2986−2994.

(16) Shaw, J. B.; Lin, T. Y.; Leach, F. E., 3rd; Tolmachev, A. V.; Tolic, N.; Robinson, E. W.; Koppenaal, D. W.; Pasa-Tolic, L. *J. Am. Soc. Mass Spectrom.* **2016**, *27* (12), 1929−1936.

(17) Kooijman, P. C.; Nagornov, K. O.; Kozhinov, A. N.; Kilgour, D. P. A.; Tsybin, Y. O.; Heeren, R. M. A.; Ellis, S. R. *Sci. Rep.* **2019**, *9* (1), 8.

(18) Smith, D. F.; Kilgour, D. P.; Konijnenburg, M.; O'Connor, P. B.; Heeren, R. M. *Anal. Chem.* **2013**, *85* (23), 11180−4.

(19) Qi, Y.; Barrow, M. P.; Li, H.; Meier, J. E.; Van Orden, S. L.; Thompson, C. J.; O'Connor, P. B. *Anal. Chem.* **2012**, *84* (6), 2923−9.

(20) Stopka, S. A.; Samarah, L. Z.; Shaw, J. B.; Liyu, A. V.; Velickovic, D.; Agtuca, B. J.; Kukolj, C.; Koppenaal, D. W.; Stacey, G.; Pasa-Tolic, L.; Anderton, C. R.; Vertes, A. *Anal. Chem.* **2019**, *91* (8), 5028−5035.

(21) Schwudke, D.; Schuhmann, K.; Herzog, R.; Bornstein, S. R.; Shevchenko, A. *Cold Spring Harbor Perspect. Biol.* **2011**, *3* (9), No. a004614.

(22) Hu, C.; Duan, Q.; Han, X. *Proteomics* **2019**, No. e1900070.

(23) Ryan, E.; Reid, G. E. *Acc. Chem. Res.* **2016**, *49* (9), 1596−604.

(24) Wildburger, N. C.; Wood, P. L.; Gumin, J.; Lichti, C. F.; Emmett, M. R.; Lang, F. F.; Nilsson, C. L. *J. Proteome Res.* **2015**, *14* (6), 2511−9.

(25) Holcapek, M.; Cervena, B.; Cifkova, E.; Lisa, M.; Chagovets, V.; Vostalova, J.; Bancirova, M.; Galuszka, J.; Hill, M. *J. Chromatogr. B: Anal. Technol. Biomed. Life Sci.* **2015**, *990*, 52−63.

(26) Korte, A. R.; Yandeau-Nelson, M. D.; Nikolau, B. J.; Lee, Y. J. *Anal. Bioanal. Chem.* **2015**, *407* (8), 2301−9.

(27) Olsen, J. V.; de Godoy, L. M.; Li, G.; Macek, B.; Mortensen, P.; Pesch, R.; Makarov, A.; Lange, O.; Horning, S.; Mann, M. *Mol. Cell. Proteomics* **2005**, *4* (12), 2010−21.

(28) Makarov, A.; Denisov, E.; Lange, O.; Horning, S. *J. Am. Soc. Mass Spectrom.* **2006**, *17* (7), 977−982.

(29) Scigelova, M.; Makarov, A. *Proteomics* **2006**, *6* (Suppl 2), 16−21.

(30) Marshall, A. G.; Hendrickson, C. L.; Jackson, G. S. *Mass Spectrom. Rev.* **1998**, *17* (1), 1−35.

(31) Nikolaev, E. N.; Gorshkov, M. V.; Mordehai, A. V.; Talrose, V. L. *Rapid Commun. Mass Spectrom.* **1990**, *4* (5), 144−146.

(32) Walker, L. R.; Tfaily, M. M.; Shaw, J. B.; Hess, N. J.; Pasa-Tolic, L.; Koppenaal, D. W. *Metallomics* **2017**, *9* (1), 82−92.

(33) Zimmerman, T. A.; Monroe, E. B.; Tucker, K. R.; Rubakhin, S. S.; Sweedler, J. V. *Methods Cell Biol.* **2008**, *89*, 361−90.

(34) Hendrickson, C. L.; Quinn, J. P.; Kaiser, N. K.; Smith, D. F.; Blakney, G. T.; Chen, T.; Marshall, A. G.; Weisbrod, C. R.; Beu, S. C. *J. Am. Soc. Mass Spectrom.* **2015**, *26* (9), 1626−32.

(35) Smith, D. F.; Podgorski, D. C.; Rodgers, R. P.; Blakney, G. T.; Hendrickson, C. L. *Anal. Chem.* **2018**, *90* (3), 2041−2047.

(36) Burla, B.; Arita, M.; Arita, M.; Bendt, A. K.; Cazenave-Gassiot, A.; Dennis, E. A.; Ekroos, K.; Han, X.; Ikeda, K.; Liebisch, G.; Lin, M. K.; Loh, T. P.; Meikle, P. J.; Oresic, M.; Quehenberger, O.; Shevchenko, A.; Torta, F.; Wakelam, M. J. O.; Wheelock, C. E.; Wenk, M. R. *J. Lipid Res.* **2018**, *59* (10), 2001−2017.

(37) Xiang, X.; Grosshans, P. B.; Marshall, A. G. *Int. J. Mass Spectrom. Ion Processes* **1993**, *125* (1), 33−43.

(38) Wong, R. L.; Amster, I. J. *Int. J. Mass Spectrom.* **2007**, *265* (2−3), 99−105.

(39) Savory, J. J.; Kaiser, N. K.; McKenna, A. M.; Xian, F.; Blakney, G. T.; Rodgers, R. P.; Hendrickson, C. L.; Marshall, A. G. *Anal. Chem.* **2011**, *83* (5), 1732−6.

(40) Schuhmann, K.; Almeida, R.; Baumert, M.; Herzog, R.; Bornstein, S. R.; Shevchenko, A. *J. Mass Spectrom.* **2012**, *47* (1), 96−104.

(41) Almeida, R.; Pauling, J. K.; Sokol, E.; Hannibal-Bach, H. K.; Ejsing, C. S. *J. Am. Soc. Mass Spectrom.* **2015**, *26* (1), 133−48.

(42) Simons, B.; Kauhanen, D.; Sylvanne, T.; Tarasov, K.; Duchoslav, E.; Ekroos, K. *Metabolites* **2012**, *2* (1), 195−213.

(43) Velickovic, D.; Chu, R. K.; Carrell, A. A.; Thomas, M.; Pasa-Tolic, L.; Weston, D. J.; Anderton, C. R. *Anal. Chem.* **2018**, *90* (1), 702−707.

(44) Spraggins, J. M.; Rizzo, D. G.; Moore, J. L.; Rose, K. L.; Hammer, N. D.; Skaar, E. P.; Caprioli, R. M. *J. Am. Soc. Mass Spectrom.* **2015**, *26* (6), 974−85.

(45) Hendrickson, C. L.; Beu, S. C.; Blakney, G. T.; Kaiser, N. K.; McIntosh, D. G.; Quinn, J. P.; Marshall, A. G. In Optimized cell geometry for Fourier transform ion cyclotron resonance mass spectrometry, *Proceedings of the 57th ASMS Conference on Mass Spectrometry and Allied Topics, Philadelphia, PA*, May 31 to June 4; Philadelphia, PA, 2009.

(46) Chen, T.; Beu, S. C.; Kaiser, N. K.; Hendrickson, C. L. *Rev. Sci. Instrum.* **2014**, *85* (6), 066107.

(47) Belov, M. E.; Ellis, S. R.; Dilillo, M.; Paine, M. R. L.; Danielson, W. F.; Anderson, G. A.; de Graaf, E. L.; Eijkel, G. B.; Heeren, R. M. A.; McDonnell, L. A. *Anal. Chem.* **2017**, *89* (14), 7493−7501.

(48) Blakney, G. T.; Hendrickson, C. L.; Marshall, A. G. *Int. J. Mass Spectrom.* **2011**, *306* (2−3), 246−252.

(49) Xian, F.; Hendrickson, C. L.; Blakney, G. T.; Beu, S. C.; Marshall, A. G. *Anal. Chem.* **2010**, *82* (21), 8807−12.

(50) Chambers, M. C.; Maclean, B.; Burke, R.; Amodei, D.; Ruderman, D. L.; Neumann, S.; Gatto, L.; Fischer, B.; Pratt, B.; Egertson, J.; Hoff, K.; Kessner, D.; Tasman, N.; Shulman, N.; Frewen, B.; Baker, T. A.; Brusniak, M. Y.; Paulse, C.; Creasy, D.; Flashner, L.; Kani, K.; Moulding, C.; Seymour, S. L.; Nuwaysir, L. M.; Lefebvre, B.; Kuhlmann, F.; Roark, J.; Rainer, P.; Detlev, S.; Hemenway, T.; Huhmer, A.; Langridge, J.; Connolly, B.; Chadick, T.; Holly, K.; Eckels, J.; Deutsch, E. W.; Moritz, R. L.; Katz, J. E.; Agus, D. B.;

MacCoss, M.; Tabb, D. L.; Mallick, P. *Nat. Biotechnol.* **2012**, *30* (10), 918−20.

(51) Race, A. M.; Styles, I. B.; Bunch, J. *J. Proteomics* **2012**, *75* (16), 5111−2.

(52) Husen, P.; Tarasov, K.; Katafiasz, M.; Sokol, E.; Vogt, J.; Baumgart, J.; Nitsch, R.; Ekroos, K.; Ejsing, C. S. *PLoS One* **2013**, *8* (11), No. e79736.

(53) Spraggins, J. M.; Djambazova, K. V.; Rivera, E. S.; Migas, L. G.; Neumann, E. K.; Fuetterer, A.; Suetering, J.; Goedecke, N.; Ly, A.; Van de Plas, R.; Caprioli, R. M. *Anal. Chem.* **2019**, *91* (22), 14552−14560.

(54) Campos, A. M.; Maciel, E.; Moreira, A. S.; Sousa, B.; Melo, T.; Domingues, P.; Curado, L.; Antunes, B.; Domingues, M. R.; Santos, F. *J. Cell. Physiol.* **2016**, *231* (5), 1024−32.

(55) Guo, S.; Wang, Y.; Zhou, D.; Li, Z. *Sci. Rep.* **2015**, *4*, 5959.

(56) Ide, Y.; Waki, M.; Hayasaka, T.; Nishio, T.; Morita, Y.; Tanaka, H.; Sasaki, T.; Koizumi, K.; Matsunuma, R.; Hosokawa, Y.; Ogura, H.; Shiiya, N.; Setou, M. *PLoS One* **2013**, *8* (4), No. e61204.

(57) Harbige, L. S.; Sharief, M. K. *Br. J. Nutr.* **2007**, *98* (Suppl 1), S46−53.

(58) Vance, J. E.; Tasseva, G. *Biochim. Biophys. Acta, Mol. Cell Biol. Lipids* **2013**, *1831* (3), 543−54.

(59) Kim, W. S.; Weickert, C. S.; Garner, B. *J. Neurochem.* **2008**, *104* (5), 1145−66.

(60) Smith, D. F.; Kharchenko, A.; Konijnenburg, M.; Klinkert, I.; Pasa-Tolic, L.; Heeren, R. M. *J. Am. Soc. Mass Spectrom.* **2012**, *23* (11), 1865−72.

(61) Estrada, R.; Yappert, M. C. *J. Mass Spectrom.* **2004**, *39* (4), 412−22.

(62) Fuchs, B.; Schiller, J.; Suss, R.; Schurenberg, M.; Suckau, D. *Anal. Bioanal. Chem.* **2007**, *389* (3), 827−34.